Celastrol induced weight loss is driven by hypophagia and independent from UCP1

Katrin Pfuhlmann[1,2,3,4], Sonja C. Schriever[1,2,4], Peter Baumann[1,2,3,4], Dhiraj G. Kabra[4,5], Luke Harrison[1,2,3,4], Sithandiwe E. Mazibuko-Mbeje[2,4,6], Raian E. Contreras[1,2,3,4], Eleni Kyriakou[7,8], Stephanie E. Simonds[9], Tony Tiganis[9], Michael A. Cowley[10], Stephen C. Woods[11], Martin Jastroch[2,4], Christoffer Clemmensen[2,4], Meri De Angelis[12], Karl-Werner Schramm[12], Michael Sattler[7,8], Ana C. Messias[7,8], Matthias H. Tschöp[2,3,4], and Paul T. Pfluger[1,2,4]

1 Research Unit Neurobiology of Diabetes, Helmholtz Zentrum München, 85764 Neuherberg, Germany.

2 Institute for Diabetes and Obesity, Helmholtz Zentrum München, 85764 Neuherberg, Germany.

3 Division of Metabolic Diseases, Technische Universität München, 80333 Munich, Germany.

4 German Center for Diabetes Research (DZD), 85764 Neuherberg, Germany.

5 Institute for Clinical Biochemistry and Pathobiochemistry, German Diabetes Center, Heinrich Heine University, Leibniz Center for Diabetes Research, 40225 Düsseldorf, Germany.

6 Biomedical Research and Innovation Platform, South African Medical Research Council, 7505 Tygerberg, South Africa.

7 Institute of Structural Biology, Helmholtz Zentrum München, 85764 Neuherberg, Germany.

8 Biomolecular NMR and Center for Integrated Protein Science Munich at Department Chemie, Technische Universität München, 85747 Garching, Germany.

9 Department of Biochemistry and Molecular Biology, Monash University, Victoria 3800, Australia.

10 Department of Physiology, Monash University, Victoria 3800, Australia.

Diabetes Publish Ahead of Print, published online August 28, 2018

11 Psychiatry and Behavioral Neuroscience, Metabolic Diseases Institute, University of Cincinnati College of Medicine, Cincinnati, OH, USA.

12 Molecular EXposomics, Helmholtz Zentrum München, 85764 Neuherberg, Germany.

Contact information:

Dr. Paul T. Pfluger, Research Unit NeuroBiology of Diabetes, Institute for Diabetes and Obesity

Helmholtz Zentrum München GmbH

Ingolstädter Landstraße 1

85764 Neuherberg, Germany

Telefon +49 (0) 89 3187 2104 (Pfluger)

paul.pfluger@helmholtz-muenchen.de

Word count: 4723

Number of figures: 4 plus 5 supplementary figures

Number of tables: 0 plus 2 supplementary tables

Abbreviations: BAT, brown adipose tissue; DIO, diet-induced obese; iWAT, inguinal white adipose tissue; MBH, mediobasal hypothalamus; PTP1B, protein tyrosine phosphatase 1 B; UCP1, uncoupling protein 1

Abstract

Celastrol, a plant-derived constituent of traditional Chinese medicine, has been proposed to offer significant potential as an anti-obesity drug. However, the molecular mechanism for this activity is unknown. We show that the weight-lowering effects of celastrol are driven by decreased food consumption. While young Lep^{ob} mice respond with a decrease in food intake and body weight, adult Lep^{db} and Lep^{ob} mice are unresponsive to celastrol, suggesting that functional leptin signaling in adult mice is required to elicit celastrols' catabolic actions. It has been previously reported that one of celastrol's targets is protein tyrosine phosphatase 1 (PTP1B), a leptin negative-feedback regulator. However, we found that global PTP1B KO and WT mice have comparable weight loss and hypophagia when treated with celastrol. Increased levels of uncoupling protein 1 (UCP1) in subcutaneous white and brown adipose tissue suggest celastrol-induced thermogenesis as a further mechanism. However, diet-induced obese UCP1 WT and KO mice have comparable weight loss upon celastrol treatment, and celastrol treatment has no impact on energy expenditure under ambient housing or thermoneutral conditions. Overall, our results suggest that celastrol-induced weight loss is hypophagia driven and, age-dependently, mediated by functional leptin signaling. Our data encourage reconsideration of therapeutic anti-obesity strategies built upon leptin sensitization.

Introduction

Extracts of celastrol, a pentacyclic triterpenoid naturally occurring in the Chinese Thunder God vine *Tripterygium wilflordii*, are used in traditional Chinese medicine to treat fever, chills, joint pain and edema. Recent evidence suggests that celastrol may be a novel anti-obesity drug that mediates weight loss by acting as a leptin sensitizer (1).

Beneficial actions of chronic celastrol treatment against obesity and diabetes were first described by Jung Kim and colleagues in 2013 (2) and corroborated by Weisberg *et al.* (3) in 2016, who observed lower body weight (BW) and blood glucose levels in leptin receptor-deficient Lep^{db} mice after treatment with 1 or 3 mg celastrol/kg BW, respectively. Because a single acute administration of intraperitoneal celastrol (3 mg/kg BW) improves glucose tolerance and insulin sensitivity in Lep^{db} mice compared to pair-fed Lep^{db} controls, the implication is that effects of celastrol on glucose homeostasis can be independent from the effects on body weight and body composition (3).

There are several suggested mechanisms for celastrol's effects. Using 10- to 30-fold lower doses, Liu and colleagues reported celastrol to be a potent leptin sensitizer that inhibits food intake (FI), lowers body weight and improves glucose tolerance by reducing hypothalamic endoplasmatic reticulum (ER) stress in diet-induced obese, but not in lean mice or in leptin (receptor)-deficient Lep^{ob} or Lep^{db} mice (1). Celastrol administration decreased hepatic steatosis via increased Sirt1 expression in mice (4), and this led to impaired adipocyte differentiation but increased lipolysis *in vitro* in 3T3 adipocyte cells (5). Celastrol has also been suggested to decrease body weight via the heat shock factor 1 (HSF1) - peroxisome proliferator-activated receptor gamma coactivator 1-alpha (PGC-1 α) axis and mitochondrial gene programs that lead to increased muscle and brown adipose tissue (BAT) thermogenesis and inguinal white adipose tissue (iWAT) browning (6).

Celastrol has several confirmed molecular targets. It inhibits IKKα and IKKβ kinases by binding to a Cysteine (Cys) residue in the kinase activation loop (7). Celastrol further inhibits the

interaction of heat shock protein 90 (Hsp90) with co-chaperones such as cell division cycle 37 (Cdc37) by binding to Cys residues in Cdc37 (8,9) or to the dimer interface of Hsp90 (10), thereby destabilizing the Hsp90-Cdc37-IKK complex and inhibiting IKK signaling. Additionally, celastrol has been found to directly inhibit proteasome activity (11) and to activate HSF1 and induce the heat shock response (12,13), but the molecular mechanisms are not known. Leptin-sensitizing properties of celastrol have been attributed to a decrease in ER stress, but direct molecular underpinnings remain elusive (1).

Our goal was to interrogate celastrol-induced weight loss by assessing celastrol's leptin-sensitizing molecular mechanism as well as its thermogenic potential. Special emphasis was given to the roles of protein tyrosine phosphatase (PTP) 1B (PTP1B) as a negative regulator of leptin action, and to uncoupling protein 1 (UCP1) as a main driver for brown/beige fat thermogenesis. Our focus on PTP1B was driven by the following rationale: A recent experiment using triterpenoids reported inhibitory activity of celastrol towards several protein phosphatases including PTP1B (14); and PTP1B is a known feedback regulator of insulin and leptin signalling via dephosphorylation of Janus kinase 2 (JAK2) (15), of the insulin receptor (IR) and of insulin receptor substrate 1 (IRS1) (16). Our focus on UCP1 was driven by a recent report that attributed the weight-lowering effects of celastrol to the transcriptional activation of UCP1 with increased BAT activation, iWAT browning and elevated energy expenditure (6).

Research design and methods

Animals

C57BL/6J mice were obtained from Janvier Labs (Saint-Berthevin Cedex, France). UCP1 KO, Lep^{ob} and Lep^{db} mice on a C57BL/6J genetic background were originally provided from Jackson Laboratory (strain names: B6.129-Ucp1tm1Kz/J; B6.Cg-Lepob/J/+; BKS.Cg-Dock7m +/+ Leprdb/J; Maine, USA). Global PTP1B KO mice (B6.129S4-$Ptpn1^{tm1Bbk}$/Mmjax) were a kind

gift of Prof. Melanie Brinckmann (Helmholtz-Zentrum für Infektionsforschung GmbH, Braunschweig, Germany). All studies were performed in male mice. All mice were maintained on a 12-h dark-light cycle and had free access to diet and water. Mice were fed normal rodent chow (Altromin, #1314) or 58% high-fat diet (HFD) (Research diets, D12331). Celastrol (BOC Science, Shirley, NY, USA, #34157-83-0) was dissolved in pure DMSO and diluted with PBS to a final concentration of 0.02 mg/ml in 1% DMSO for injections. 100 µg/kg BW of celastrol or PBS with 1% DMSO as vehicle was injected in a similar volume. HFD-fed DIO mice and chow-fed mice were injected intraperitoneally (ip). UCP1 WT and KO mice, Lep^{ob} WT and KO mice, Lep^{db} WT and KO mice and PTP1B WT and KO mice were injected subcutaneously (sc). Celastrol injections took place 1-2 h before dark onset. HFD-fed mice were injected with 100 µg/kg BW celastrol or vehicle 1-2 h before sacrifice. Mice were distributed into treatment groups based on their starting body weight in order to assure an equal distribution of starting body weights, allowing for better dissection of the effects of longitudinal treatments on body weight. *In vivo* experiments were performed without blinding of the investigators. All studies were based on power analyses to assure adequate sample sizes, and approved by the State of Bavaria, Germany.

Body composition and indirect calorimetry

Fat and lean masses were assessed using nuclear magnetic resonance (NMR) technology (EchoMRI, Houston, TX, USA). Energy expenditure, locomotor activity and exact food intake measurements were analyzed by a combined indirect calorimetry system (TSE System, Bad Homburg, Germany). Mice were acclimatized to the calorimetry system for at least 24 h before data collection for 3 d and 21 h at 23°C. To assess the impact of celastrol on basal metabolic rates and maximum respiration, housing temperatures were changed to 30°C for 17 h. Mice were subsequently injected with 0.5 µg/g BW norepinephrine (Sigma-Aldrich, St. Louis, Missouri, USA) in 0.9% NaCl 2.5 h after light onset, and assessed for the maximum increase in

energy expenditure observed within 1 h. We determined the basal metabolic rates of vehicle and celastrol-treated mice housed at 30°C by averaging energy expenditure values from 4.5 to 6.5 h after light onset, a period when mice displayed the lowest daily physical activity. For the measurement of maximum respiration, one mouse had to be excluded due to a missed norepinephrine injection, and one mouse had to be excluded from food intake analyses due to spillage.

Glucose-tolerance tests

Mice were treated for 6 d with celastrol (100 µg/kg body weight) or vehicle and then subjected to a glucose-tolerance test (GTT) on Day 7. After 6 h of fasting, 1.5 g glucose/kg body weight was injected ip and tail blood glucose was measured using a handheld glucometer (Freestyle freedom Lite, Abbott Diabetes Care, Alameda, CA, USA) before (0 min) and 15, 30, 60 and 120 min after glucose injection.

RNA isolation and qPCR analysis

RNA was isolated from tissue using a commercially available kit (Macherey-Nagel, Düren, Germany). Equal amounts of RNA were transcribed to cDNA using the QuantiTect Reverse Transcription kit (Qiagen, Hilden, Germany). Gene expression was analyzed using custom-made primers (Sigma, St Louis, MO, USA), TaqMan probes (Thermo Fischer Scientific, Inc., Rockford, IL USA) and SYBR Green™ or TaqMan mastermix (Applied Biosystem, Carlsbad, CA, USA). Gene expression was evaluated using the delta-delta Ct method and *Hprt* was used as the housekeeping gene. Primer pairs and TaqMan probes used are listed in the supplementary tables. Ct values for hypothalamic inflammatory markers were between 32 and 36.

Western blotting and densitometric analyses

RIPA buffer containing protease and phosphatase inhibitor cocktail (Thermo Fisher Scientific Inc., Rockford, IL, USA) and 1 mM phenyl-methane-sulfonyl fluorid (PMSF) were used for protein extraction. A Trans Blot Turbo transfer apparatus (Biorad, Hercules, CA, USA) transferred proteins from precast poly acrylamide gels (Biorad, Hercules, CA, USA) to nitrocellulose membranes. Membranes were incubated with anti-pSTAT3^{T705} (rabbit polyclonal, 1:2500, Cat #9145), anti-STAT3 (mouse monoclonal, 1:2500, Cat #9139), anti-STAT5, (rabbit polyclonal, 1:1000, Cat #9363), anti-UCP1 (rabbit monoclonal, 1:1000, Cat #14670) and anti-β-Actin (rabbit polyclonal, 1:20000, Cat #4970). All antibodies were purchased form Cell Signaling Technology (Cell Signaling, Danvers, MA, USA). Membranes were detected on a LiCor Odyseey instrument (Lincoln, NE, USA) using ECL (Biorad, Hercules, California, USA), and densitometric quantifications were performed using internal LiCor Odyssey software.

Immunohistochemistry

After perfusion of mice with PBS and a chilled 4% solution of paraformaldehyde in 0.1 M PBS, brains were extracted and incubated in fixative overnight on a shaker at 4°C. After incubation for 24-48 h with 30% sucrose in 0.1 M TBS at 4°C, brains were frozen at -20°C, coronally cut in a cryostat into 30 µm sections and stored in a cryoprotectant solution containing glycerol, ethylene glycol and sucrose dissolved in TBS. Stainings were performed with free-floating slices, and were started by applying 2-h blocking in a buffer containing 0.25% gelatin and 0.5% Triton X 100 in 1x TBS. Primary anti-pSTAT3 goat (1:200, Santa Cruz, #sc7993) and anti-POMC (1:500, Phoenix, H-029-30) were diluted in blocking buffer and incubated overnight at 4°C. After several washing steps, Biotin-SP-conjugated AffiniPure Fab Fragment goat anti-mouse IgG (H+L) (1:500, Jackson Immunoresearch, #115-069-033) was added to the slices in TBS for 1 h. After washing, strepavidin-Alexa Fluor 555 conjugate (1:500, Life Technologies, #115-067-033) and Alexa Fluor 488 goat anti-rabbit IgG (H+L) antibody (1:500, Life Technologies, #A11008) were added in TBS for 1 h and washed afterwards several times. Z-

stack images were captured by a Leica TCS SP8 microscope. Stack and overlay pictures were created using ImageJ 1.47v software. The ARC was defined in each slice by orienting on DAPI and POMC staining as well as on the Allen brain Atlas (http://mouse.brain-map.org/static/atlas). Green and red staining as well as green-red co-localizations in the ARC were counted, and pSTAT3 and POMC double-positive cells were normalized to the total number of POMC positive cells in the ARC. Total numbers of pSTAT3 and POMC positive cells were normalized to ARC area.

Liquid chromatography quantitative time of flight mass spectrometry (LC-Q-TOF-MS)

Celastrol was dissolved to a concentration of 0.08 mg/mL in the following solutions: (a) pure DMSO, (b) 50% DMSO in PBS, (c) 10% DMSO in PBS, (d) 5% DMSO in PBS or (e) 45% 2-Hydroxypropyl-beta-cyclodextrin (cyclodextrin) containing 0.8 µl DMSO/ml in PBS, (f) 45% cyclodextrin in PBS. The celastrol solutions were then further diluted 1:400 and 1:800 with a mixture of H_2O:CH_3CN (1:1). Glycyrrhetinic acid was used as internal standard and dissolved in methanol to reach a concentration of 100 ng/µl. To each diluted solution, glycyrrhetinic acid was added to reach a final concentration of 2 ng/µl (dilution 1:400) and 1 ng/µl (dilution 1:800). All solutions containing the internal standard were subsequently analyzed with a nanoAcquity UPLC system (Waters, Milford, USA) that was connected to a quadrupole time-of-flight (Q-TOF2) mass spectrometer (Waters Micromass, Manchester, UK). Compound separation was carried out on a BEH C18 micro-scale column (300 µm i.d. × 150 mm length, 1.7 µm particle size; Waters, Milford, MA, USA). The gradient HPLC method used water (A) and acetonitrile (B) each containing 0.1% formic acid (v/v) as mobile phases. The gradient was as follows: 60% B held for 2 min, and then increasing to 70% B in 1 min, kept at 70% B for 7 min. The gradient then returned to the initial condition of 60% B over 1 min which was held for 4 min to allow for equilibration before the next injection. Additional parameters were as follows: column temperature, 40°C; flow rate, 5 µl/min; injection volume, 5 µl. The Q-TOF was operated in

electrospray negative ionization mode. The microchannel plate (MCP) detector potential was 2100 V. The capillary extraction voltage and cone voltage were 2.5 kV and 70 V, respectively. High purity nitrogen was used as desolvation gas and auxiliary gas, and argon was used as collision gas. The desolvation gas temperature and flow rate were 120°C and 200 l/h, respectively. The cone gas flow rate was 50 l/h. The source temperature was 100°C. The collision energy was 25 eV. The instrumentation ran in full-scan mode with the Q-TOF data collected over the range 100 – 1000 m/z with a scan time of 2 s and inter scan time of 0.1 s. Data acquisition and processing were performed on the QuanLynx Application Manager software (Waters-Micromass, Manchester, UK). The stability of celastrol was calculated based on the ratio between peak area internal standard (IS) divided by peak area celastrol. Every experiment was repeated in duplicates.

^{1}H-NMR

A 10 mM (4.5g/ml) stock solution of celastrol in pure DMSO-d6 was prepared. From this stock the following solutions were prepared: (a) celastrol at a final concentration of 177.5 µM (0.08 mg/ml) in DMSO-d6; (b) celastrol in PBS with 50% DMSO-d6; (c) celastrol in PBS with 10% DMSO-d6 and (d) celastrol in PBS with 5% DMSO-d6. The sample of 177.5 µM celastrol in DMSO-d6 was used as reference where the solubility of celastrol is considered 100%. Subsequently, aliquots of all samples were incubated at 37 °C, and measured at day 0, 7 and 14. Samples were then subjected to one-dimensional (1D) ^{1}H-NMR at 37°C on a Bruker 600 MHz spectrometer equipped with a cryogenic QCI-probehead (^{1}H, ^{31}P, ^{13}C, ^{15}N) equipped with Z-gradients. 1D ^{1}H experiments were performed using a WATERGATE pulse sequence with 19k time domain and 128 scans using 177.5 µM celastrol samples in 100% DMSO-d6 and in PBS buffer pH 7.4 and 5%/10%/50% DMSO-d6. The solubility of celastrol was calculated based on the ratio between peak intensity of the aromatic proton 6 of celastrol in pure DMSO-d6 at time 0 divided by peak intensity of the same celastrol proton in PBS solution.

Statistical Analyses

Statistical analyses were performed using GraphPad Prism (GraphPad Software, Inc. La Jolla, CA, USA) or SPSS (IBM, Armonk, NY, USA). Untailed student's t-test or two-way ANOVA with Bonferroni's post test were applied to compare differences between phenotypes. Combined indirect calorimetry measurements were assessed by Analysis of Co-Variance (ANCOVA), using lean and fat mass as covariates. P-values lower than 0.05 were considered significant. Significances were indicated as follow: $*^{/+}p < 0.05$, $**^{/++}p < 0.01$, $***^{/+++}p < 0.001$, $****^{/++++}p<0.0001$. All results are presented as means +/- SEM.

Results

Celastrol has compromised stability in aqueous solutions

To evaluate celastrol as weight loss agent in DIO mice, we first aimed to determine a formulation suitable for chronic *in vivo* injection studies. NMR revealed highest stability and solubility when celastrol was dissolved in pure DMSO-d6 (Supplementary Fig. 1a, Supplementary Table 1), but decreasing stability and solubility when celastrol was dissolved under aqueous buffer conditions (PBS) with decreasing amounts of 50%, 10% or 5% DMSO-d6 (Supplementary Fig. 1b-d, Supplementary Table 1) at 37 °C and over a time period of 14 days. Notably, despite adequate solubility at day 0, there was a dramatic drop in peak intensity and the appearance of new resonances for celastrol dissolved in PBS with 50% DMSO-d6 after 7 and 14 days of incubation (Supplementary Fig. 1e-g). The emergence of new peaks that increase in intensity over time, including in the aromatic region, points to reactions of celastrol with other molecules in solution, most likely with molecules resulting from the reaction of DMSO in aqueous solution (17). When celastrol was further diluted in PBS to 10% or 5% DMSO-d6, the

occurrence of these additional peaks diminished, but the reduction of the parent compound was confounded with poor solubility. LC-MS analyses confirmed the reduction in solubility as well as the poor stability of celastrol in aqueous buffers (Supplementary Table 2). Notably, by adding the complexing agent beta-cyclodextrin (45% in PBS), we could increase the stability of celastrol incubated for 7 or 14 days at 37°C. Overall, however, the best solvent for celastrol appears to be 100% DMSO, all tested aqueous solutions either showed decreased stability at days 7 and 14 and/or decreased solubility at day 0. Pure DMSO is nevertheless toxic to mice, especially when given chronically. Accordingly, to minimize toxic side effects, we daily prepared fresh celastrol dissolved in 1% DMSO for all injection studies.

Celastrol induces hypophagia and weight loss

To identify the mechanism(s) by which celastrol achieves weight loss, we administered celastrol (100 μg/kg, ip) once daily for 6 days and observed significantly reduced body weight, fat mass and lean mass in HFD-fed diet-induced obese (DIO, Fig. 1a,b, Supplementary Fig. 2a; age 36 ± 1 weeks; 32 weeks of HFD feeding) and chow-fed mice (Fig. 1c,d, Supplementary Fig. 2b; age 36 ± 1 weeks). Celastrol treatment reduced food intake in DIO mice (Fig. 1e) and there was a trend in the same direction in chow-fed mice (Fig. 1f). The decrease in FI in DIO mice was delayed, with maximum efficacy occurring 9 to 12 h after celastrol administration (Supplementary Fig. 2c-e), suggesting a celastrol-dependent alteration of gene expression. Decreased respiratory exchange ratios and locomotory patterns were temporally correlated with reduced food intake (Supplementary Fig. 2f-h). Overall, we observed proportionally greater weight loss in direct linear correlation to body weight in all mice tested, regardless of chow or HFD feeding (Fig. 1g); i.e. heavier mice lost the most weight, while lean mice lost little to no weight.

Celastrol-induced weight loss requires functional leptin signaling in adult mice

Contrary to reports using 10- to 30-fold higher doses (2,3), but consistent with the findings of Liu and colleagues, celastrol (100 μg/kg) did not decrease BW, fat nor lean mass in 8-wk-old chow-fed leptin receptor-deficient Lep^{db} mice (Fig. 2a-c, Supplementary Fig. 3a). Functionality of celastrol was confirmed by a reduction of BW (Fig. 2a) as well as fat and lean mass (Fig. 2c) in age-matched chow-fed lean C57Bl/6J (WT) controls with a mean BW of 23.5 g (Supplementary Fig. 3a). Similarily, celastrol had no weight loss efficacy in 14-wk-old chow-fed leptin-deficient Lep^{ob} mice, but decreased BW, fat and lean mass in age-matched chow-fed WT controls (Fig. 2d,e,f) with a BW of 30.6 g (Supplementary Fig. 3b). Celastrol treatment for 6 days further improved glucose tolerance in chow-fed WT but not in celastrol-injected Lep^{ob} mice (Fig. 2g,h).

To assess whether effects of 100 μg/kg celastrol on BW, FI and body composition are indeed strictly leptin-dependent, we administered vehicle or leptin to a group of young (age 6 wk) chow-fed Lep^{ob} mice (Supplementary Fig. 3c). In contrast to what occurred in aged mice, there was reduced weight gain in Lep^{ob} mice treated with celastrol, compared to vehicle-treated Lep^{ob} mice, and this was reflected by significantly reduced fat and lean mass (Supplementary Fig. 3d,e). These celastrol-treated Lep^{ob} mice also had reduced food intake compared to vehicle-treated controls (Supplementary Fig. 3f). Our data are thus consistent with an earlier report that shows temporary weight reduction in young Lep^{ob} mice (1), indicating that celastrol's leptin sensitizing activity may be age-dependent. Alternatively, since young Lep^{db} mice had no weight loss in response to celastrol treatment (Fig. 2b and (1)), it appears plausible that celastrol may temporarily increase the constitutive activity of the LepRb, or its affinity for alternative cytokines (1). .

To identify celastrol's first-order targets, we next assessed key hypothalamic signaling networks that orchestrate glucose and energy homeostasis. Surprisingly, celastrol administration to DIO mice (age 36 ± 1 wk, 32 wk on HFD) significantly increased Agouti-related protein (AgRP) mRNA expression while having no effect on mRNA expression of other neuropeptides and

components of leptin and melanocortin signaling (Supplementary Fig. 4a,b). Moreover, celastrol had little impact on mRNA levels of genes involved in hypothalamic ER stress and hypothalamic inflammation (Supplementary Fig. 4c). The nearly identical and somewhat paradoxical increase in hypothalamic AgRP expression after celastrol treatment has already been reported by Liu *et al.* (1), which makes it unlikely to be a coincidence or artefact. Rather, it might be a counterregulatory response to the negative energy balance of celastrol-treated mice. Overall, however, the reason for the increase in AgRP mRNA levels remains elusive.

Celastrol administration did not lead to an additional activation of leptin-responsive neurons in the hypothalamus, as revealed by similar numbers of phosphorylated signal transducer and activator of transcription 3 (pSTAT3)-positive POMC neurons (Fig. 3a,b). Nevertheless and consistent with the data of Liu *et al.* (1), phosphorylation levels of the leptin target STAT3 (Fig. 3c,d), as well as basal STAT3 and STAT5 protein levels (Fig. 3c,e), were elevated in celastrol-injected mice. These data imply that celastrol may either drive the further activation of leptin-responsive POMC neurons, or induce the recruitment and activation of additional LepRb-expressing neuronal subpopulations in the hypothalamus. The excacerbation of leptin signaling in leptin-responsive neurons could be facilitated by a direct celastrol-driven disruption of JAK-STAT feedback inhibition.

Celastrol-induced weight loss is unperturbed by global PTP1B deletion

JAK-STAT feedback inhibition is mediated by protein tyrosine phosphatases (PTPs), which are long-recognized anti-obesity drug targets (18). PTP1B was the first PTP linked to leptin signaling (19), and the PTP1B inhibitor and leptin sensitizer trodusquemine shares structural similarities with celastrol (20). We thus assessed whether celastrol mediates leptin resensitization via inhibition of PTP1B. We first assessed celastrol-induced weight loss in PTP1B WT and KO littermates with similar initial body weights (Supplementary Fig. 4d) that were exposed to the chow diet (age 22 ± 7 wk). Chow-fed PTP1B KO mice had more weight

loss upon celastrol treatment than WT littermates (Fig. 3f), and this was accompanied by non-significant decreases in fat and lean mass in PTP1B KO mice, and a significant loss of lean mass in WT mice (Fig. 3g). Similarly, when the same cohort of mice was subsequently exposed to HFD for 10 wk, celastrol induced weight loss in both PTP1B WT and KO mice (Fig. 3h), and this was largely explained by concomitant decreases in fat and lean mass (Fig. 3i). Notably, in contrast to earlier studies (21) (22) reporting protection from DIO in PTP1B-deficient mice, we observed similar body weights; i.e., there was a similar propensity for DIO in WT and PTP1B littermates exposed to 10 wk of HFD (Supplementary Fig. 4e).

Celastrol-induced weight loss is independent from UCP1-driven thermogenesis

We next assessed whether celastrol can facilitate weight loss via uncoupling protein 1 (UCP1)-mediated mitochondrial uncoupling in adipose tissue. Consistent with a recent report (6), celastrol led to up-regulated gene expression of medium-chain acyl-CoA dehydrogenase (*Mcad*) and *Ucp1* in BAT, and of heat shock factor protein-1 (*Hsf1*) and uncoupling protein-1 (*Ucp1*) in iWAT (Fig. 4a), as well as to higher UCP1 protein levels in BAT (Fig. 4b). However, transcription of *Pgc1-*α and key thermogenic genes was unaffected in iWAT and BAT (Supplementary Fig. 5a,b). Celastrol had also no cell-autonomous thermogenic effects on C2C12 muscle cells *in vitro* (Supplementary Fig. 5c,d), and did not induce mitochondrial genes or genes involved in non-shivering thermogenesis in skeletal muscle *in vivo* (Supplementary Fig. 5e,f).

Despite elevated UCP1 levels in iWAT and BAT, there was no impact of celastrol treatment in DIO mice on energy expenditure, basal metabolic rate or maximal norepinephrine-induced respiration under ambient housing or thermoneutral conditions of 23°C and 30°C, respectively, (Fig. 4c,d; age 24 wk, 20 wk HFD exposure). Similarly, pair-feeding vehicle-treated DIO mice to the average food consumption of celastrol-treated DIO mice resulted in the same decrease in body weight (Fig. 4e, Supplementary Fig. 5g) as well as in fat and lean mass (Fig. 4f), compared

to ad libitum-fed vehicle-treated DIO mice (age 16 wk, 12 wk on HFD). These data suggest that the reduction of food intake (Fig. 4g) is likely the main driver for celastrol-induced loss of lean mass, thus arguing against putative toxic effects of celastrol on lean mass. Moreover, DIO UCP1-deficient mice and isogenic DIO WT mice had comparably decreased BW, fat mass and FI in response to celastrol administration (Fig. 4h-j, Supplementary Fig. 5h; age 44 ± 4 wk, 34 wk of HFD). Collectively, these results strongly argue that celastrol-induced BW reduction is not mediated by UCP1-mediated mitochondrial uncoupling and thermogenesis.

Discussion

Ideal treatment strategies against obesity will entail both a reduction in food intake and the expenditure of excessive energy via thermogenesis. While the former is a centrally mediated process, the latter results from increased heat production by peripheral thermogenic tissues such as white or brown adipose tissue and skeletal muscle. Celastrol has recently emerged as a promising anti-obesity drug that can induce both hypophagia due to unprecedented *in vivo* leptin resensitization properties (1), as well as to iWAT browning and BAT UCP1 levels (6). Our results are consistent with these reports, revealing a concomitant increase in UCP1 levels in iWAT and BAT of mice treated with celastrol, and celastrol-induced weight loss that is due to a partially leptin-dependent decrease in food consumption. However, follow-up experiments revealed comparable BW loss and hypophagia in UCP1 KO and WT mice treated with celastrol, implying that UCP1-mediated thermogenesis is not a major driver for the body weight-lowering effects of celastrol.

The lack of celastrol-induced weight loss in adult Lep^{ob} and Lep^{db} mice suggests that celastrol-induced reduction of food intake is strictly leptin-dependent. Nevertheless, we found considerable celastrol-induced hypophagia and weight loss in 6-wk-old leptin-deficient mice. This is consistent with a previous report of metabolic improvements of celastrol administered at

a higher dose (1 mg/kg BW, ip) in 8-wk-old leptin receptor-deficient Lep^{db} mice (2), or with a temporary weight loss in young Lep^{ob} mice which nevertheless disappeared after prolonged low-dose celastrol treatment (1). These data highlight the plurality of celastrol's catabolic actions which may include the sensitization of CNS LepRb signaling as well as non-leptin-driven mechanisms. In this context, one should further note that our current definition of leptin resistance is largely based on the failure of exogenous leptin to reduce food intake and body weight. On a molecular level, however, the definition of leptin resistance largely remains an enigma, with one recent report even questioning the existence of resistance against endogenous leptin signaling (23).

A putative molecular player in the development of leptin resistance is leptin negative feedback regulator PTP1B. Celastrol was recently reported to have direct inhibitory activity against PTP1B in an *in vitro* phosphatase assay (14). However, we found celastrol-induced weight loss in both WT and global PTP1B deficient mice, indicating that there are PTP1B-independent mechanisms of celastrol action. However, the high sequence homology between PTP1B and T-cell PTP (TCPTP) makes it plausible that TCPTP is also a target of celastrol. This also resonates with recent studies demonstrating that only a concomitant deletion of PTP1B and TCPTP signaling in POMC neurons blocks hypothalamic leptin actions on iWAT browning and BAT activation (24). Accordingly, our findings of iWAT browning and BAT UCP1 expression may point to a concomitant inhibition of both PTP1B and TCPTP by celastrol. Compensatory hypothalamic TCPTP signaling could explain the unperturbed weight loss efficacy of celastrol in global PTP1B KO mice. However, whether celastrol indeed inhibits TCPTP remains to be tested by *in vitro* binding assays or *in vivo* murine loss-of-function models.

Hypophagia as the main driver for celastrol-induced weight loss implicates the CNS as the primary celastrol target tissue. Specifically, CNS centers governing leptin-dependent ingestive behaviors appear to be the most promising sites of celastrol action. Future studies should delineate the relative contribution of these CNS areas for celastrol action. Celastrol's chemical

instability in aqueous buffers, especially in the presence of DMSO to increase its solublity, may however complicate chronic studies on the catabolic actions of celastrol in the CNS. Such studies on CNS celastrol actions may be directed towards leptin-melanocortin signaling in hypothalamic AgRP and/or POMC neurons, but neurocircuitry outside the hypothalamus could be of equal importance. Future studies will help distinguish celastrol's direct effects on the CNS from indirect effects caused by celastrol-induced weight loss, or from potentially direct effects against peripheral targets such as pancreatic beta-cells (3).

In summary, our results in UCP1 loss-of-function models argue against celastrol-induced iWAT or BAT browning and UCP1-dependent or independent thermogenesis (25-28) as being the primary cause of the observed weight loss due to celastrol. Rather, the major impact of celastrol on weight loss appears to be driven via the CNS control of food intake. Age or a putative sensitization of LepRb signaling appear to be key factors for the lack of catabolic actions of celastrol in adults, but for normal weight loss in young Lep^{ob} mice. However, the mode of action and exact role of leptin signaling remain elusive. Overall, we corroborate the considerable potential of celastrol as an anti-obesity drug. A pair-feeding study revealed that the loss of body adiposity, and minor loss of lean mass after celastrol treatment was solely driven by a reduction in food intake. Accordingly, celastrol appears safe and efficacious in preclinical models of obesity as well as in lean mice. These discoveries encourage reconsideration of leptin sensitizers as drugs against metabolic dysfunction. Moreover, by delineating the molecular action of celastrol, we may be able to shed new light on the enigma that is leptin resistance.

Acknowledgements

K.P., S.C.S., P.B., D.G.K., L.H., R.E.C., C.C. and P.T.P. performed in vivo experiments in mice. K.P. and P.B. conducted immunohistochemical stainings. K.P. performed qPCRs and Western Blot analyzes. S.E.M. and M.J. performed in vitro experiments in C2C12 cells. E.K., A.C.M. and M.S. performed 1D ^{1}H-NMR experiments. M.D.A. and K.W.S. conducted LC-Q-

TOF-MS measurements. K.P., S.C.S., D.G.K., E.K., S.C.W., S.E.S., C.C., T.T., M.D.A., K.W.S., M.A.C., M.H.T., and P.T.P. designed experiments, analyzed and interpreted the results. K.P., E.K., A.C.M., S.C.W., T.T., M.A.C., M.H.T., P.T.P. prepared the manuscript. S.C.S., A.C.M., M.H.T. and P.T.P. developed the conceptual framework of this study. We further thank Emily V. Baumgart, Heidi Hofmann, Laura Sehrer, and Luisa Müller for their skillful technical assistance. P.T.P., the guarantor of the study, had full access to all the data and takes responsibility for the integrity of the data and the accuracy of the data analysis. This work was supported in part by the Marie Skłodowska Curie training network 'ChroMe' (grant H2020-MSCA-ITN-2015-675610; R.C., M.H.T., P.T.P.), by the Alexander von Humboldt Foundation (M.H.T.), by the Helmholtz Alliance ICEMED-Imaging and Curing Environmental Metabolic Diseases (S.C.S., M.H.T.), by the Helmholtz Portofolio Program “Metabolic Dysfunction” (M.S., M.H.T.), by an IMF Diabetes Portfolio Grant (A.C.M., M.S.), by the NHMRC Australia (M.A.C. and S.E.S.) and National Heart Foundation of Australia (S.E.S.), by the Helmholtz-Israel-Cooperation in Personalized Medicine (P.T.P.), by the Helmholtz Initiative for Personalized Medicine (iMed; M.H.T.), and through the Initiative and Networking Fund of the Helmholtz Association.

Competing Interests

Matthias Tschöp is a scientific advisor to Novo Nordisk and ERX.

References

1. Liu J, Lee J, Salazar Hernandez MA, Mazitschek R, Ozcan U. Treatment of Obesity with Celastrol. Cell. Elsevier Inc; 2015 May 21;161(5):999–1011.

2. Kim JE, Lee MH, Nam DH, Song HK, Kang YS, Lee JE, et al. Celastrol, an NF-κB Inhibitor, Improves Insulin Resistance and Attenuates Renal Injury in db/db Mice. Nerurkar PV, editor. PLoS ONE. 2013 Apr 26;8(4):e62068–11.

3. Weisberg S, Leibel R, Tortoriello DV. Proteasome inhibitors, including curcumin, improve pancreatic β-cell function and insulin sensitivity in diabetic mice. Nutr Diabetes.

2016 Apr 25;6:e205.

4. Zhang Y, Geng C, Liu X, Li M, Gao M, Liu X, et al. Celastrol ameliorates liver metabolic damage caused by a high-fat diet through Sirt1. Mol Metab. 2017 Jan;6(1):138–47.

5. Choi SK, Park S, Jang S, Cho HH, Lee S, You S, et al. Cascade regulation of PPARγ(2) and C/EBPα signaling pathways by celastrol impairs adipocyte differentiation and stimulates lipolysis in 3T3-L1 adipocytes. Metab Clin Exp. 2016 May;65(5):646–54.

6. Ma X, Xu L, Alberobello AT, Gavrilova O, Bagattin A, Skarulis M, et al. Celastrol Protects against Obesity and Metabolic Dysfunction through Activation of a HSF1-PGC1α Transcriptional Axis. Cell Metabolism. 2015 Oct 6;22(4):695–708.

7. Lee JH, Koo TH, Yoon H, Jung HS, Jin HZ, Lee K, et al. Inhibition of NF-kappa B activation through targeting I kappa B kinase by celastrol, a quinone methide triterpenoid. Biochem Pharmacol. 2006 Nov 15;72(10):1311–21.

8. Sreeramulu S, Gande SL, Göbel M, Schwalbe H. Molecular mechanism of inhibition of the human protein complex Hsp90-Cdc37, a kinome chaperone-cochaperone, by triterpene celastrol. Angewandte Chemie International Edition. WILEY-VCH Verlag; 2009;48(32):5853–5.

9. Jiang F, Wang H-J, Bao Q-C, Wang L, Jin Y-H, Zhang Q, et al. Optimization and biological evaluation of celastrol derivatives as Hsp90-Cdc37 interaction disruptors with improved druglike properties. Bioorg Med Chem. 2016 Nov 1;24(21):5431–9.

10. Peng B, Gu Y-J, Wang Y, Cao F-F, Zhang X, Zhang D-H, et al. Mutations Y493G and K546D in human HSP90 disrupt binding of celastrol and reduce interaction with Cdc37. FEBS Open Bio. 2016 Jul;6(7):729–34.

11. Yang H, Landis-Piwowar KR, Chen D, Milacic V, Dou QP. Natural compounds with proteasome inhibitory activity for cancer prevention and treatment. Curr Protein Pept Sci. 2008 Jun;9(3):227–39.

12. Westerheide SD, Bosman JD, Mbadugha BNA, Kawahara TLA, Matsumoto G, Kim S, et al. Celastrols as inducers of the heat shock response and cytoprotection. J Biol Chem. American Society for Biochemistry and Molecular Biology; 2004 Dec 31;279(53):56053–60.

13. Trott A, West JD, Klaić L, Westerheide SD, Silverman RB, Morimoto RI, et al. Activation of heat shock and antioxidant responses by the natural product celastrol: transcriptional signatures of a thiol-targeted molecule. Mol Biol Cell. American Society for Cell Biology; 2008 Mar;19(3):1104–12.

14. Scott LM, Chen L, Daniel KG, Brooks WH, Guida WC, Lawrence HR, et al. Shp2 protein tyrosine phosphatase inhibitor activity of estramustine phosphate and its triterpenoid analogs. Bioorg Med Chem Lett. 2011 Jan;21(2):730–3.

15. Myers MP, Andersen JN, Cheng A, Tremblay ML, Horvath CM, Parisien JP, et al. TYK2 and JAK2 are substrates of protein-tyrosine phosphatase 1B. J Biol Chem. American Society for Biochemistry and Molecular Biology; 2001 Dec 21;276(51):47771–4.

16. Salmeen A, Andersen JN, Myers MP, Tonks NK, Barford D. Molecular basis for the dephosphorylation of the activation segment of the insulin receptor by protein tyrosine

phosphatase 1B. Mol Cell. 2000 Dec;6(6):1401–12.

17. Lee Y, Lee C, Yoon J. Kinetics and mechanisms of DMSO (dimethylsulfoxide) degradation by UV/H2O2 process. Water Research. 2004 May;38(10):2579–88.

18. Ukkola O, Santaniemi M. Protein tyrosine phosphatase 1B: a new target for the treatment of obesity and associated co-morbidities. J Intern Med. 2002 Jun;251(6):467–75.

19. Zabolotny JM, Bence-Hanulec KK, Stricker-Krongrad A, Haj F, Wang Y, Minokoshi Y, et al. PTP1B Regulates Leptin Signal Transduction In Vivo. Dev Cell. Elsevier; 2002 Apr 1;2(4):489–95.

20. Lantz KA, Hart SGE, Planey SL, Roitman MF, Ruiz-White IA, Wolfe HR, et al. Inhibition of PTP1B by Trodusquemine (MSI-1436) Causes Fat-specific Weight Loss in Diet-induced Obese Mice. Obesity. Nature Publishing Group; 2009 Nov 13;18(8):1516–23.

21. Elchebly M, Payette P, Michaliszyn E, Cromlish W, Collins S, Loy AL, et al. Increased insulin sensitivity and obesity resistance in mice lacking the protein tyrosine phosphatase-1B gene. Science. 1999 Mar 5;283(5407):1544–8.

22. Brommage R, Desai U, Revelli J-P, Donoviel DB, Fontenot GK, Dacosta CM, et al. High-throughput screening of mouse knockout lines identifies true lean and obese phenotypes. Obesity (Silver Spring). Wiley-Blackwell; 2008 Oct;16(10):2362–7.

23. Ottaway N, Mahbod P, Rivero B, Norman LA, Gertler A, D'Alessio DA, et al. Diet-induced obese mice retain endogenous leptin action. Cell Metabolism. 2015 Jun 2;21(6):877–82.

24. Dodd GT, Decherf S, Loh K, Simonds SE, Wiede F, Balland E, et al. Leptin and Insulin Act on POMC Neurons to Promote the Browning of White Fat. Cell. 2015 Jan;160(1-2):88–104.

25. Kusminski CM, Bickel PE, Scherer PE. Targeting adipose tissue in the treatment of obesity-associated diabetes. Nat Rev Drug Discov. 2016 Sep;15(9):639–60.

26. Kazak L, Chouchani ET, Jedrychowski MP, Erickson BK, Shinoda K, Cohen P, et al. A Creatine-Driven Substrate Cycle Enhances Energy Expenditure and Thermogenesis in Beige Fat. Cell. Elsevier Inc; 2015 Oct 22;163(3):643–55.

27. Long JZ, Svensson KJ, Bateman LA, Lin H, Kamenecka T, Lokurkar IA, et al. The Secreted Enzyme PM20D1 Regulates Lipidated Amino Acid Uncouplers of Mitochondria. Cell. Elsevier Inc; 2016 Jul 14;166(2):424–35.

28. Keipert S, Kutschke M, Ost M, Schwarzmayr T, van Schothorst EM, Lamp D, et al. Long-Term Cold Adaptation Does Not Require FGF21 or UCP1. Cell Metabolism. 2017 Aug 1;26(2):437–446.e5.

Figures

Fig. 1 | Celastrol decreases body weight in chow- and HFD-fed mice.

(a,b) DIO mice (age 36 ± 1 wk, exposed to HFD for 32 wk) treated daily with celastrol (100 µg/kg body weight (BW); intraperitoneal injections (ip); n=7) or vehicle (n=7) for 6 d displayed BW loss **(a)** and fat and lean mass loss **(b)**.

(c,d) Chow-fed C57BL/6J mice (age 36 ± 1 wk) were treated daily with 100 µg celastrol/kg BW or vehicle (ip) for 6 days. **(c)** BW changes and **(d)** changes in body composition in chow-fed mice (n=8).

(e,f) Mean daily food intake (FI) was assessed over a period of 6 days in **(e)** DIO mice (7 cages) and **(f)** chow-fed C57BL/6J mice (2 cages) treated daily with celastrol (100 µg/kg BW) or vehicle (ip).

(g) Correlation of BW changes on study day 6 and intitial BW at day 0 in mice injected with celastrol (100 µg/kg BW; n=53).

Two-Way ANOVA with Bonferroni post-hoc tests were applied for a and c. Unpaired student t-tests were used for statistical anaylses of figures b, d, e. Linear regression was applied for g. Means ± SEM; *P<0.05; ***P<0.001; ****P<0.0001.

Fig. 2 | Celastrol-induced weight loss is leptin dependent.

(a-c) BW changes in chow-fed and age-matched **(a)** lean C57Bl/6J (WT; age 8 wk) and **(b)** leptin-receptor deficient obese Lep^{db} mice treated subcutaneously (sc) with celastrol (100 µg/kg BW/d; WT: n=4, Lep^{db}: n=4) or vehicle (WT: n=4, Lep^{db}: n=4) for 6 days, and **(c)** changes in body composition.

(d-h) Changes in BW **(d,e)**, body composition **(f)** and glucose tolerance **(g,h)** in male chow-fed and age-matched C57Bl/6J (WT; age 14 ± 2 wk) and leptin deficient obese Lep^{ob} mice fed with chow diet and treated with celastrol (100 µg/kg BW/d, sc; WT: n=8, Lep^{ob}: n=6) or vehicle (WT: n=8, Lep^{ob}: n=5-6) for 6 days**.** Mice in **(g,h)** received an intraperitoneal bolus of 2 g glucose per kg body weight (WT: n=5, Lep^{ob}: n=4).

Two-Way ANOVA with Bonferroni post-hoc tests were applied to a, b, d, e, g (left panel), h (left panel). Unpaired student t-tests were used c, f, g (right panel), h (right panel). Means ± SEM; *P<0.05; **P<0.01**;** ***P<0.001; ****P<0.0001.

Fig. 3 | Celastrol increases hypothalamic pSTAT3 as well as basal STAT3 and STAT5 protein levels but celastrol-induced weight loss is independent from PTP1B.

(a,b) Hypothalamic slices of male HFD-fed C57BL/6J mice (age 36 ± 3 wk) injected with 100 µg celastrol/kg BW/d or vehicle for 6 days (ip) were subjected to **(a)** immunostaining with anti-POMC and anti-pSTAT3 antibody (scale bar 50 µm), and assessed for the **(b**, left panel**)** percentage of pSTAT3-positive POMC cells or **(b**, right panel**)** the number of POMC or pSTAT3-positive cells per area (n=5-6).

(c-e) Western Blot **(c)** and densitometric analyses of **(d)** phosphorylated signal-transducer-and-activator of transcription-3 (pSTAT3, normalized to total STAT3) or **(e)** basal STAT3 and STAT5 (normalized to β-Actin) protein levels in hypothalami of celastrol (100 µg/kg BW/d) or vehicle treated mice (ip; n=7-8).

(f-i) Changes in BW **(f)** and body composition **(g)** in chow-fed male global PTP1B KO mice and WT littermates (age 22 ± 7 wk) treated with celastrol (100 µg/kg BW/d, ip; WT: n=6, PTP1B KO: n=5) or vehicle (WT: n=7, PTP1B KO: n=5; one vehicle injected PTP1B KO animal was identified as a significant outlier with a Grubbs test and was therefore excluded) for 7 days. Celastrol-induced weight loss **(h)** and body composition changes **(i)** were further tested in male global PTP1B KO mice and WT littermates acutely exposed to 10 wk of HFD and one week of daily celastrol injections (100 µg/kg BW/d, ip; WT: n=7, PTP1B KO: n=5) or vehicle (WT: n=7, PTP1B KO: n=5).

Unpaired students t-tests were used for b, d, e, g, i. Two-Way ANOVA with Bonferroni post-hoc tests were applied to f, h. Means ± SEM; *P<0.05; **P<0.01**;** ***P<0.001; ****p<0.0001.

Fig. 4 | Celastrol decreases body weight independent from UCP1 and has no effect on energy expenditure.

(a) mRNA levels of genes involved in browning, β-oxidation and heat shock response in brown adipose tissue (BAT) and inguinal white adipose tissue (iWAT) of celastrol vs. vehicle-treated DIO mice (n=7, 6 day ip injection, 100 µg/kg). Uncoupling protein 1 (*Ucp1*), medium chain acyl CoA dehydrogenase (*Mcad*), heat shock factor 1 (*Hsf 1*).

(b) Protein levels of UCP1 in brown adipose tissue of celastrol vs. vehicle-treated (ip) DIO mice, depicted by Western Blot and densitometry analyses (n=7-8, 6 days ip injection, 100 µg celastrol/kg BW).

(c) Unperturbed energy expenditure at ambient room temperature in HFD-fed male DIO mice injected daily (indicated by arrows) with 100 µg celastrol/kg BW or vehicle for 4 days (n=6).

(d) Additional indirect calorimetry measurements of celastrol (100 µg/kg BW/d, ip) and vehicle injected mice further revealed unchanged basal metabolic rates (BMR) and maximal respiratory capacities (Max. Resp.) after a single injection of norepinephrine (0.5 µg/g BW) under thermoneutral conditions (n=7).

(e-g) Pair-feeding of HFD-fed and vehicle-treated male DIO mice (age 16 wk) to the amount of food consumed by celastrol-treated (100 µg/kg BW/d) DIO mice led to a similar reduction in body weight **(e)** as well as fat and lean mass **(f)** compared to ad libitum-fed and vehicle-treated DIO mice, indicating that the reduction of food intake **(g**; 3-5 cages**)** is solely responsible for celastrol-induced weight loss.

(h-j) DIO WT and UCP1 KO mice (age 44 ± 4 wk) subjected to 100 µg celastrol/kg BW/d (sc, WT: n=7, KO: n=7) or vehicle (WT: n=7, KO: n=7) for 6 days displayed BW loss **(h)**, fat and lean mass loss **(i)** and decreased daily food intake **(j**; 3-7 cages**)**.

Unpaired students t-tests were used for a, b, c (right panel), d, i, j. Two-Way ANOVA with Bonferroni post-hoc tests was applied for e, g, h. ANCOVA was applied on c (right panel), f.

Means ± SEM; *P<0.05, **P<0.01**,** ****P<0.0001 Celastrol vs. Vehicle (a,b,e,g,h,I,j) or Vehicle vs. Vehicle Pair-fed (f); $^{++}$P<0.01, $^{+++}$P<0.001, $^{++++}$P<0.0001 Vehicle vs. Vehicle Pair-fed (e,g).

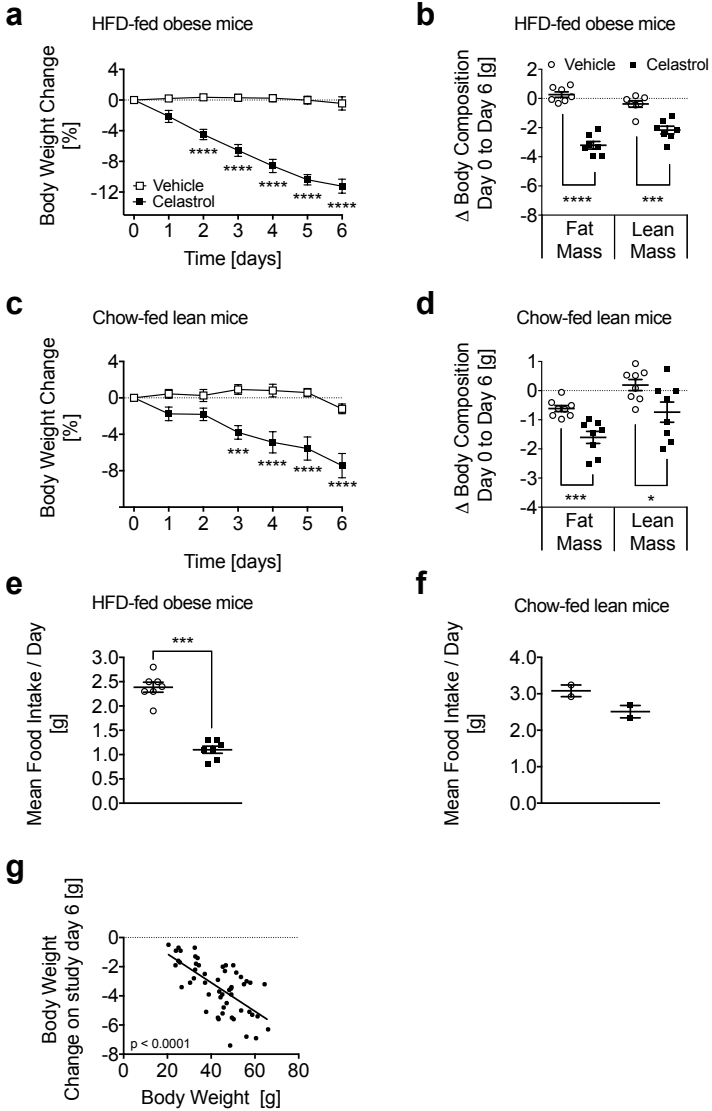
a
HFD-fed obese mice
Body Weight Change [%]
Vehicle
Celastrol
Time [days]
b
HFD-fed obese mice
Vehicle
Celastrol
Δ Body Composition Day 0 to Day 6 [g]
Fat Mass
Lean Mass
c
Chow-fed lean mice
Body Weight Change [%]
Time [days]
d
Chow-fed lean mice
Δ Body Composition Day 0 to Day 6 [g]
Fat Mass
Lean Mass
e
HFD-fed obese mice
Mean Food Intake / Day [g]
f
Chow-fed lean mice
Mean Food Intake / Day [g]
g
Body Weight Change on study day 6 [g]
p < 0.0001
Body Weight [g]

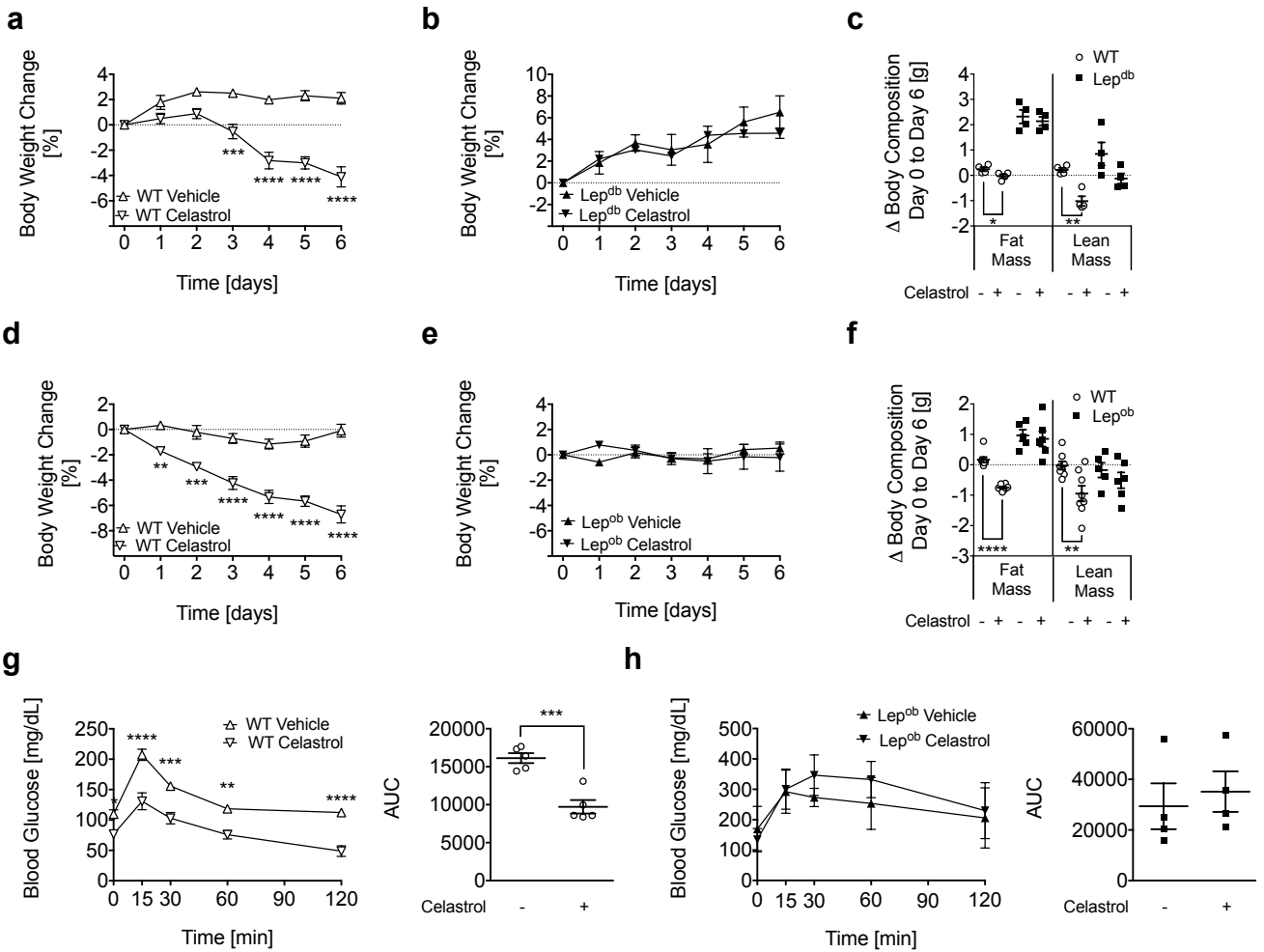
a
Body Weight Change [%]
WT Vehicle
WT Celastrol
Time [days]
b
Body Weight Change [%]
Lepdb Vehicle
Lepdb Celastrol
Time [days]
c
Δ Body Composition Day 0 to Day 6 [g]
WT
Lepdb
Fat Mass
Lean Mass
Celastrol - + - + - + - +
d
Body Weight Change [%]
WT Vehicle
WT Celastrol
Time [days]
e
Body Weight Change [%]
Lepob Vehicle
Lepob Celastrol
Time [days]
f
Δ Body Composition Day 0 to Day 6 [g]
WT
Lepob
Fat Mass
Lean Mass
Celastrol - + - + - + - +
g
Blood Glucose [mg/dL]
WT Vehicle
WT Celastrol
Time [min]
AUC
Celastrol - +
h
Blood Glucose [mg/dL]
Lepob Vehicle
Lepob Celastrol
Time [min]
AUC
Celastrol - +

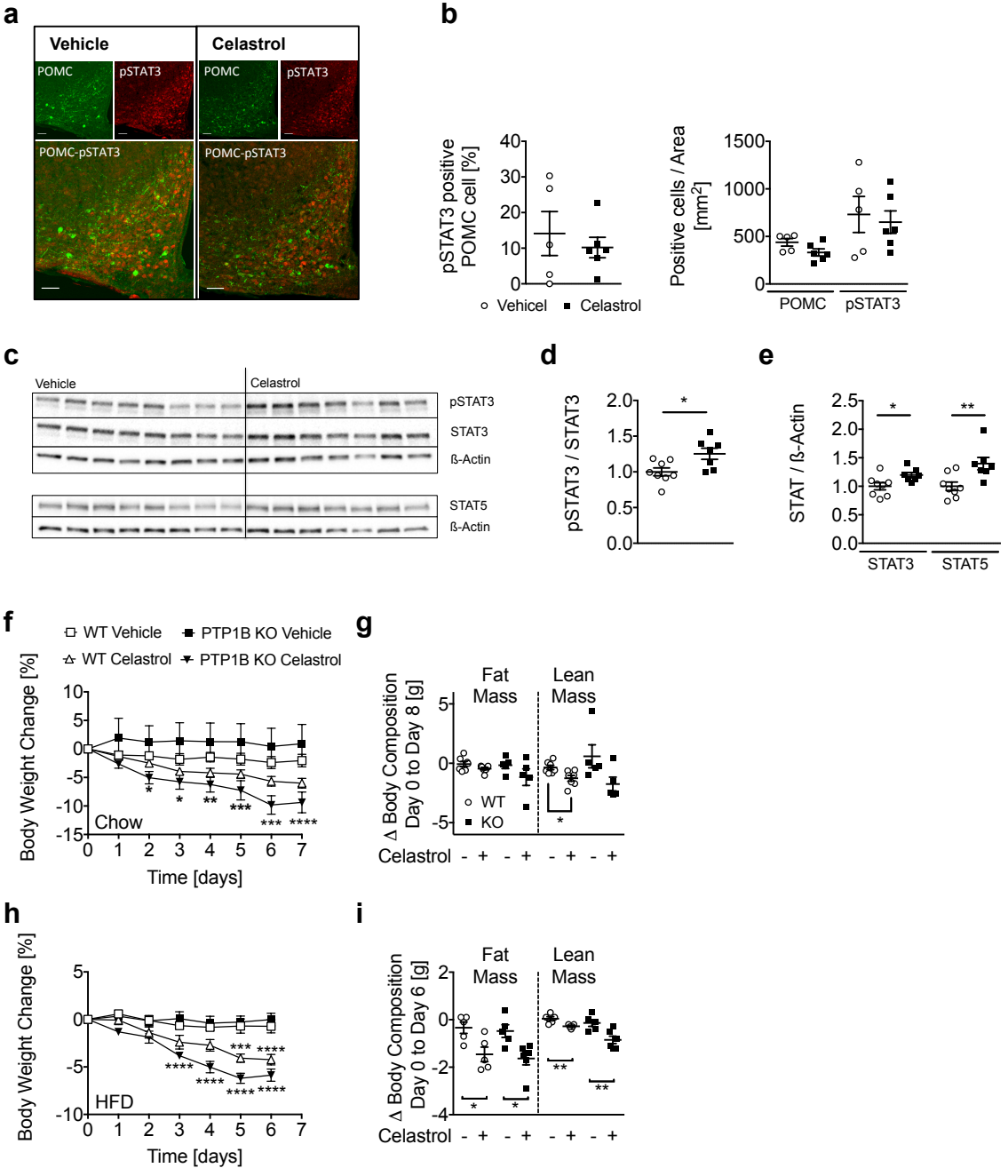
a
Vehicle
Celastrol
POMC
pSTAT3
POMC-pSTAT3
b
pSTAT3 positive POMC cell [%]
Vehicel
Celastrol
Positive cells / Area [mm²]
POMC
pSTAT3
c
Vehicle
Celastrol
pSTAT3
STAT3
ß-Actin
STAT5
ß-Actin
d
pSTAT3 / STAT3
e
STAT / ß-Actin
STAT3
STAT5
f
WT Vehicle
PTP1B KO Vehicle
WT Celastrol
PTP1B KO Celastrol
Body Weight Change [%]
Chow
Time [days]
g
Δ Body Composition Day 0 to Day 8 [g]
Fat Mass
Lean Mass
WT
KO
Celastrol
h
Body Weight Change [%]
HFD
Time [days]
i
Δ Body Composition Day 0 to Day 6 [g]
Fat Mass
Lean Mass
Celastrol

Figure 4

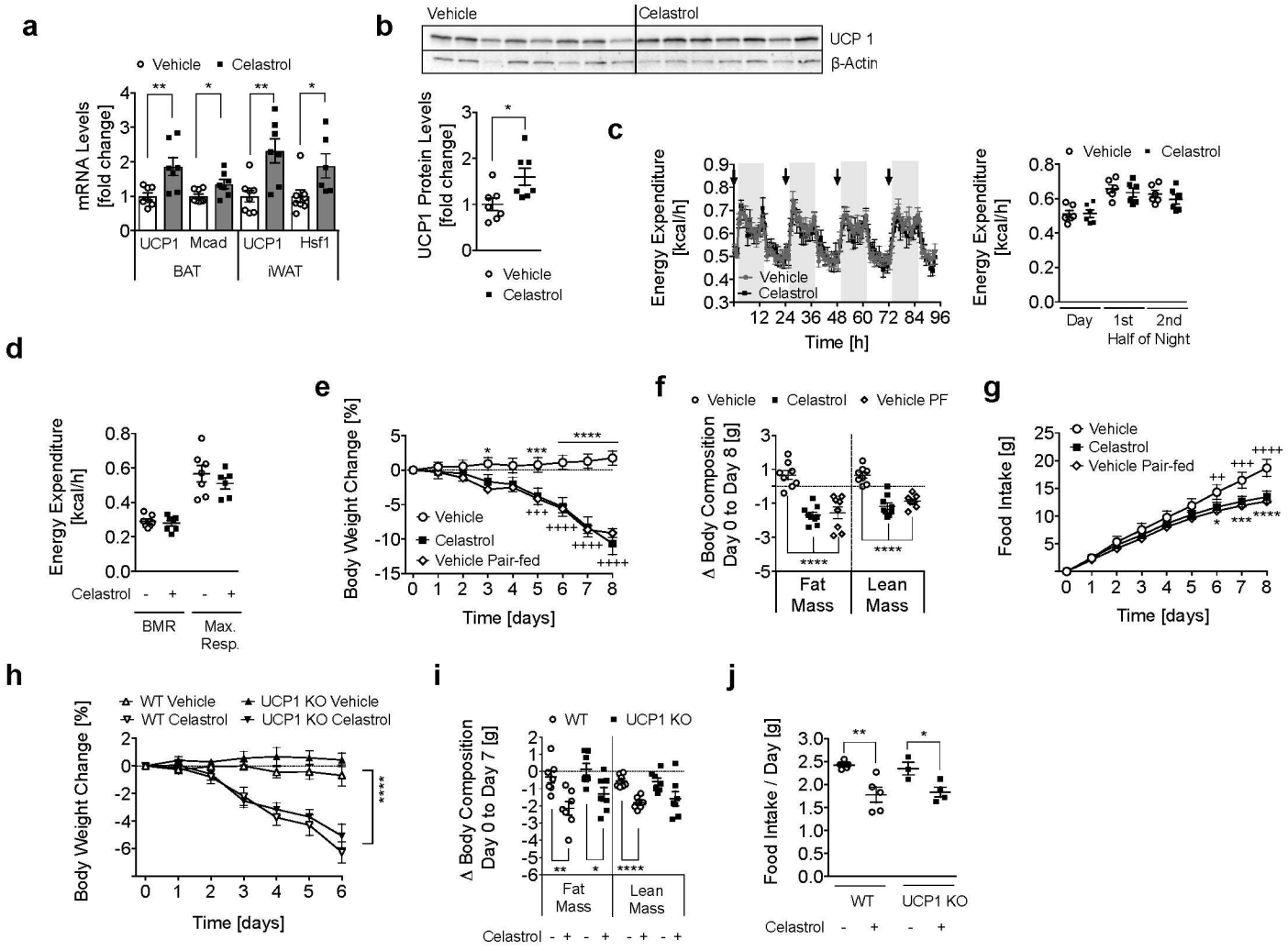
a
Vehicle
Celastrol
mRNA Levels [fold change]
UCP1
Mcad
UCP1
Hsf1
BAT
iWAT
b
Vehicle
Celastrol
UCP 1
β-Actin
UCP1 Protein Levels [fold change]
c
Energy Expenditure [kcal/h]
Time [h]
Day
1st Half of Night
2nd Half of Night
d
Energy Expenditure [kcal/h]
Celastrol
BMR
Max. Resp.
e
Body Weight Change [%]
Time [days]
Vehicle
Celastrol
Vehicle Pair-fed
f
Vehicle
Celastrol
Vehicle PF
Δ Body Composition Day 0 to Day 8 [g]
Fat Mass
Lean Mass
g
Food Intake [g]
Time [days]
h
WT Vehicle
WT Celastrol
UCP1 KO Vehicle
UCP1 KO Celastrol
Body Weight Change [%]
Time [days]
i
WT
UCP1 KO
Δ Body Composition Day 0 to Day 7 [g]
Fat Mass
Lean Mass
Celastrol
j
Food Intake / Day [g]
WT
UCP1 KO
Celastrol

Online Appendix

Supplementary Data

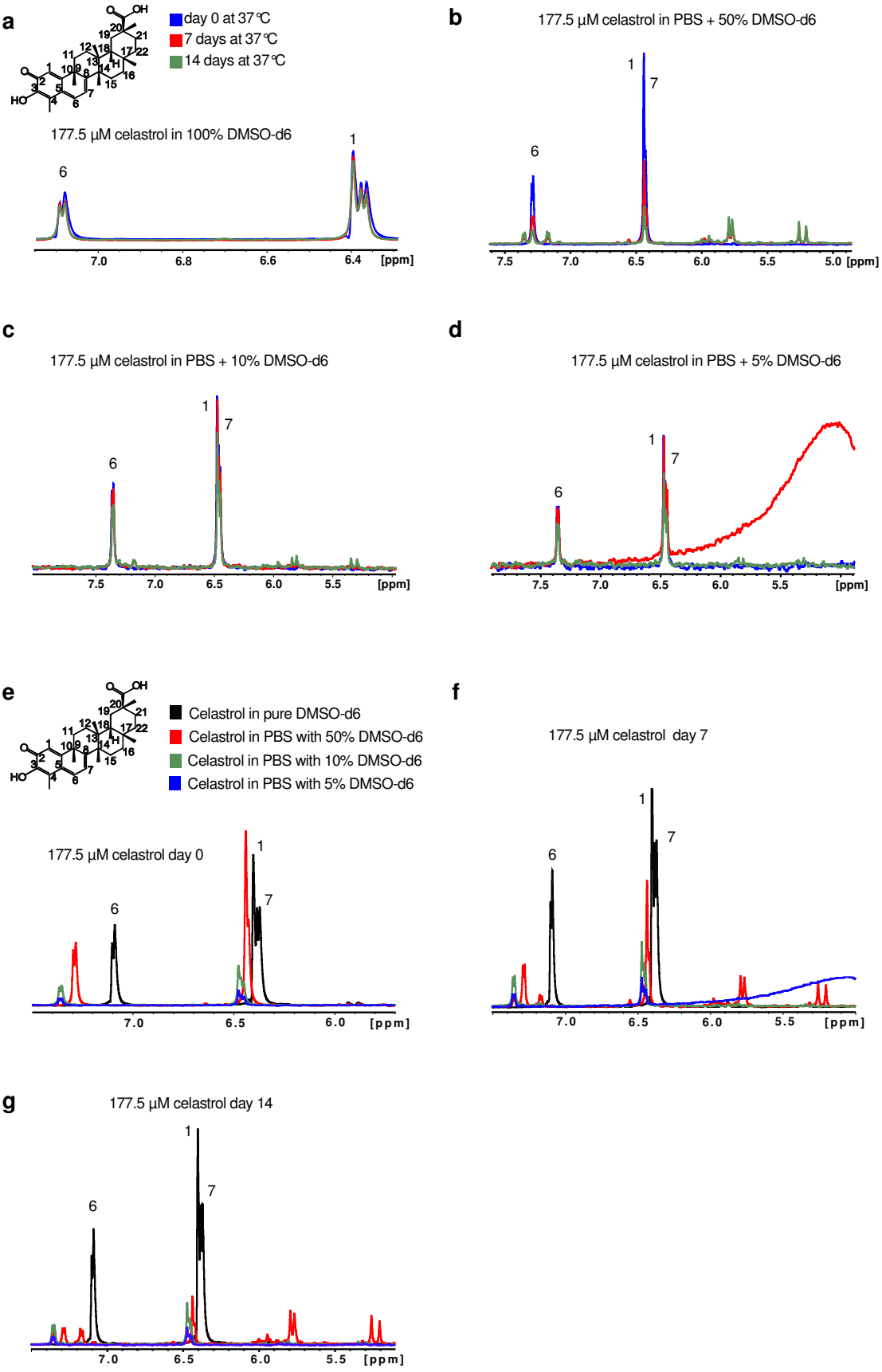

Supplementary Fig. 1 | Stability testing of celastrol in DMSO and DMSO-PBS using ^{1}H-NMR

(a-d) ^{1}H-NMR spectra of celastrol in (a) pure DMSO-d6, (b) PBS with 50% DMSO-d6, (c) PBS with 10% DMSO-d6 and (d) PBS with 5% DMSO-d6 after 0 (blue), 7 (red) and 14 (green) days of incubation at 37°C. The spectra show superimposition of the aromatic region of celastrol over time. A decrease in the intensity of the peaks indicates that the amount of soluble celastrol has decreased over time.

(e-g) ^{1}H-NMR spectra of celastrol (aromatic region) in pure DMSO-d6 (black), PBS with 50% DMSO-d6 (red), 10% DMSO-d6 (green), 5% DMSO-d6 (blue) recorded at time 0 (e), day 7 (f) and day 14 (g). A decrease in the intensity of the peaks indicates that the amount of soluble celastrol has decreased over the time.

The decrease in peak intensity of celastrol dissolved in PBS with 50% DMSO-d6 (red) (b; red spectra in (e,f,g) points to a reaction of celastrol with degradation products of DMSO, which likely appears as new peaks for reaction products between 5 and 6 ppm.

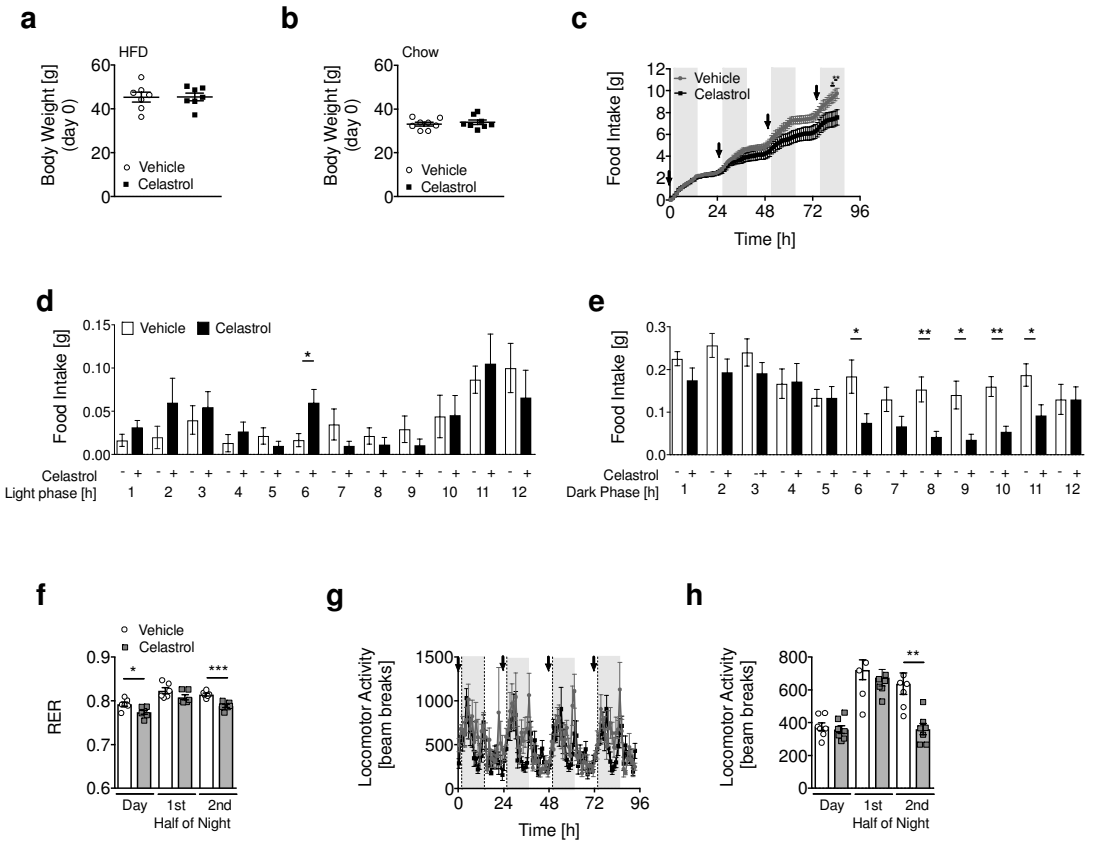

Supplementary Fig. 2 | Celastrol reduces food intake and locomotor activity in chow- and HFD-fed mice.

(a,b) Starting body weights of male HFD-fed DIO (a; n=7) and chow-fed (b; n=8) C57Bl/6J mice injected daily with 100 µg/kg BW/d celastrol or vehicle (ip).

(c-e) Cumulative food intake (c) and average (mean per animal over 3 nights, from second to fourth night) food intake in the light (d) and dark phase (e) of male DIO mice injected daily (see arrow) with 100 µg/kg BW/d celastrol or vehicle (ip) for 4 d (n=6).

(f,g) Corresponding respiratory exchange ratios (RER), average values for the light phase and the first and second half of the dark phase (3 days and 4 nights; n=6-7) (d) and locomotor activity patterns and average values for the light phase and the first and second half of the dark phase (3 days and 4 nights; n=6-7) of vehicle or celastrol-treated mice (e).

Two-Way ANOVA with Bonferroni post-hoc tests were applied on c and g (left panel). Unpaired students t-tests were applied on a, b, d, e, f and h. Means ± SEM; *P<0.05; **P<0.01; ***P<0.001.

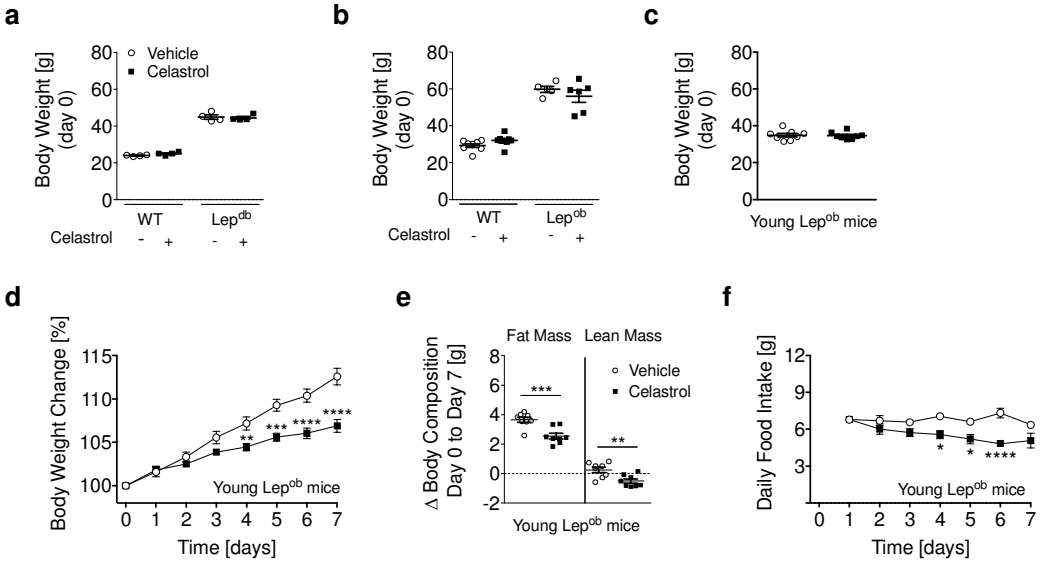

Supplementary Fig. 3 | Celastrol actions in leptin (receptor) deficient mice

(a,b) Starting body weights of male chow-fed WT or Lep^{db} mice (a; n=4; age 8 weeks) and WT or Lep^{ob} mice (b; WT: vehicle n=8, celastrol n=8; Lepob: vehicle n=5, celastrol n=6; age: 14 ± 2 wk) at day 0 of daily vehicle or celastrol (100 µg/kg BW/d, ip) injections.

(c-f) Young male, chow-fed Lep^{ob} mice (n=8) with an age of 6 wk and with similar starting body weights (c; BW day 0) were treated with vehicle or celastrol (100 µg/kg BW/d, ip) for 7 days to monitor celastrol-induced reductions in body weight (d), fat and lean mass (e) and food intake (f; n=4 cages).

Unpaired students t-tests were applied on a, b, c and e. Two-Way ANOVA with Bonferroni post-hoc tests were applied on d and f. Means ± SEM; *P<0.05; **P<0.01; ***P<0.001.

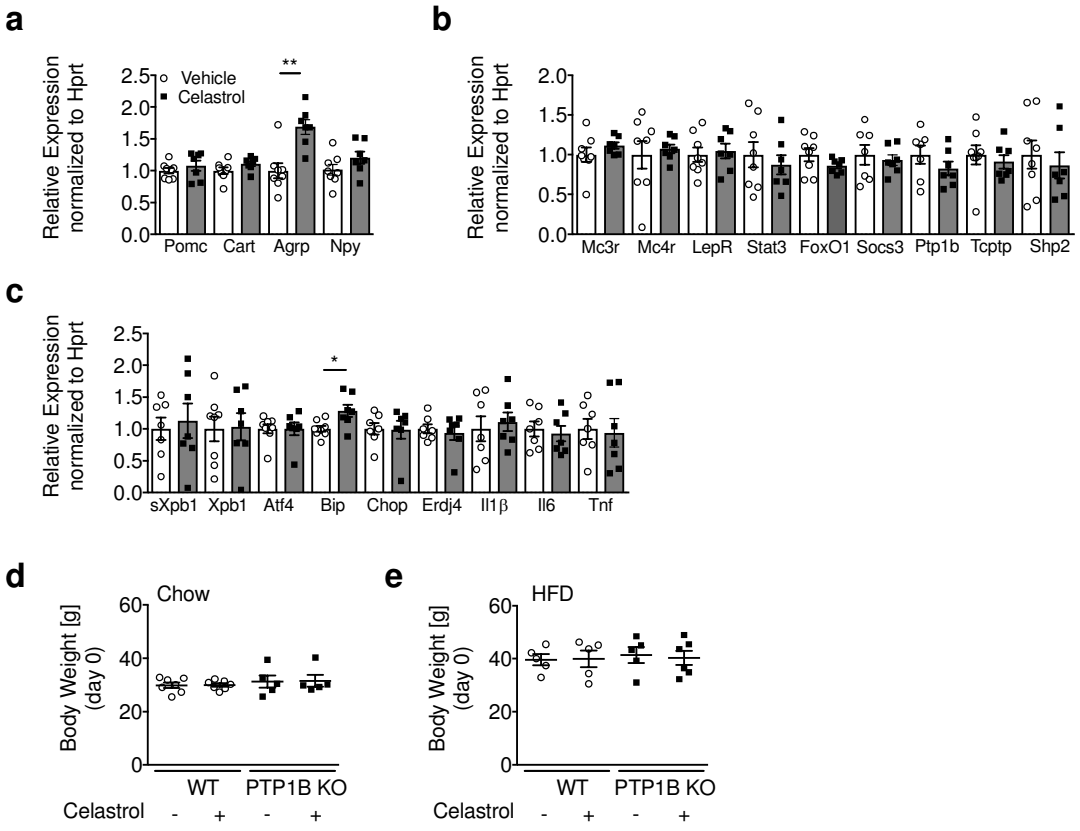

Supplementary Fig. 4 | Effect of celastrol treatment on hypothalamic inflammatory networks, leptin signaling components and genes involved in ER stress.

(a-c) Impact of celastrol (100 µg/kg BW/d for 6 d, ip, DIO mice, n=7-8) on hypothalamic mRNA levels of (a) pro-opiomelanocortin (Pomc), cocaine- and amphetamine-regulated transcript (Cart), agouti-related protein (Agrp) and neuropeptide Y (Npy); (b) genes involved in anorexigenic-, orexigenic- and leptin signaling, i.e. melanocortin-3-receptor (Mc3r), melanocortin-4-receptor (Mc4r), leptin receptor (LepR), signal-transducer-and-activator of transcription-3 (Stat3), forkhead box O1 (Foxo1), suppressor-of-cytokine signaling-3 (Socs3), protein tyrosine phosphatase 1B (Ptp1b), t-cell protein tyrosine phosphatase (Tcptp) and Src-homology 2 domain-containing phosphatase 2 (Shp2); (c) genes involved in endoplasmatic reticulum (ER) stress (spliced form of X-box binding protein 1 (sXbp1), Xbp1, activating transcription factor 4 (Atf4), binding immunoglobulin protein (Bip), CCAAT-enhancer-binding protein homologous protein (Chop), endoplasmic reticulum-localized DnaJ4 (Erdj4))

and inflammation (interleukin-1 beta (Il1β), interleukin-6 (Il6) and tumor necrosis factor (Tnf)) (n=7-8).

(d,e) Day 0 body weights at the start of seven daily vehicle or celastrol (100 µg/kg BW/d, ip) injections in male WT (vehicle & celastrol: n=7) and PTP1B KO mice (vehicle & celastrol: n=5) that were initialy fed chow diet (d; age: 22 ± 7 wk) and subsequently subjected to 8 wk of HFD feeding (e).

Unpaired students t-tests were applied on a, b, c, d, e. Means ± SEM; *P<0.05; **P<0.01; ***P<0.01; **P<0.01..

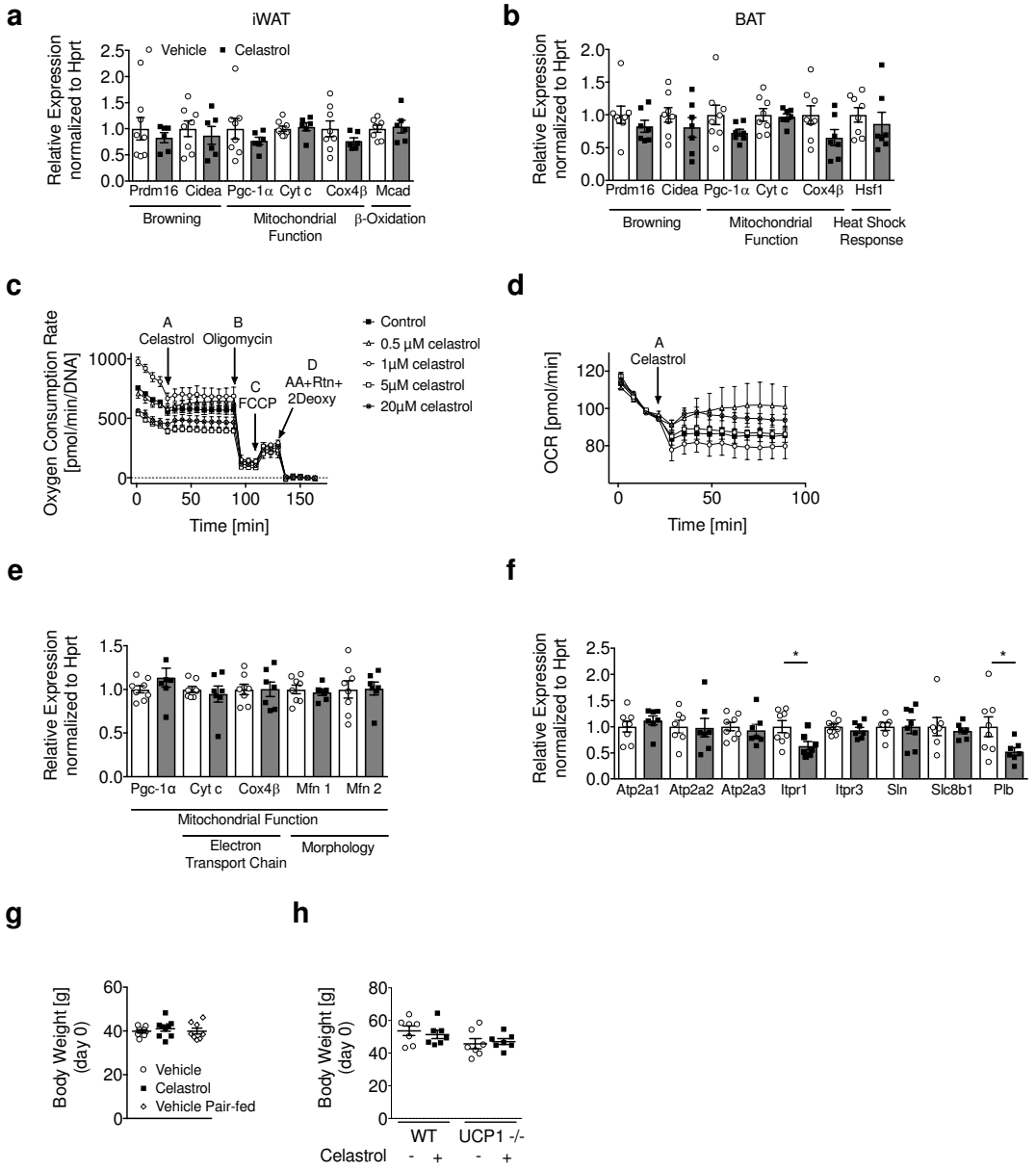

Supplementary Fig. 5 | Effect of celastrol on key regulators of adipose tissue and skeletal muscle metabolism.

(a,b) mRNA levels of genes involved in browning, mitochondrial function, β-oxidation and heat shock response in (a) inguinal white adipose tissue (iWAT) and (b) brown adipose tissue (BAT) of celastrol vs. vehicle-treated (ip) DIO mice. PR domain containing 16 (Prdm16), cell death-inducing DFFA-Like Effector A (Cidea), peroxisome proliferator-activated receptor gamma coactivator 1-alpha (Pgc-1α), cytochrome c (Cyt c), cytochrome oxidase 4 β (Cox4), medium-chain-acyl-CoA-dehydrogenase (Mcad) and heat shock factor 1 (Hsf 1) (n=6-8).

(c,d) Oxygen consumption rates (OCRs) in C2C12 cells treated with increasing amounts of celastrol. (c) Oligomycin, Carbonyl cyanide-4-(trifluoromethoxy)phenylhydrazone (FCCP) and Antimycin A (AA), Rotenone (Rtn) and 2-deoxy glucose (2Deoxy) were added to delineate the impact of celastrol on ATP synthase activity, maximum respiration and non-mitochondrial respiration, respectively. Initial differences in basal respiration result from using wells at the border vs. the inside of the plates. OCRs were (d) normalized to the value measured at the time when celastrol was added.

(e) Expression levels of genes involved in mitochondrial function; i.e. Pgc-1α, Cyt c, Cox4β, mitofusin-1 (Mfn1) and mitofusin-2 (Mfn2), in gastrocnemii of DIO mice treated with celastrol or vehicle (ip) for 6 d (n=7-8).

(f) Expression levels of sarcoplasmic reticulum genes Ca2+ ATPase transporting cardiac muscle fast twitch 1 (Atp2a1), Ca2+ ATPase transporting cardiac muscle slow twitch 2 (Atp2a2), Ca2+ ATPase transporting ubiquitous (Atp2a3), inositol 1,4,5-triphosphate receptor 1 (Itpr1), inositol 1,4,5-trisphosphate receptor 3 (Itpr3), sarcolipin (Sln), solute carrier family 8 (sodium/lithium/calcium exchanger) member B1 (Slc8b1) and phospholamban (Plb) in gastrocnemii of DIO mice treated with celastrol or vehicle (ip) for 6 d (n=8).

(g) Starting body weights of male HFD-fed DIO mice (age: 16 wk) that were subjected to daily vehicle (n=8) or celastrol (n=9; 100 µg/kg BW/d; ip) injections or to daily vehicle injections plus pair-feeding to the reduced average calorie-intake of the celastrol-treated mice (vehicle pair-fed; n=8).

(h) Starting body weights of male HFD-fed DIO WT and UCP1 KO mice (n=7; age 44 ± 4 wk) that were subjected to daily injections of vehicle or celastrol (100 µg/kg BW/d; ip).

Students t-tests were applied on a, b, e, f, g and h. Means ± SEM; *P<0.05.

Supplementary Tables

Supplementary Table 1 | Stability test for a 177.5 µM solution of celastrol in different solvents at day 0, 7 and 14 by NMR. The stability is calculated based on the ratio between peak intensity of the aromatic proton 6 of celastrol in PBS solution divided by the peak intensity of the same celastrol proton in pure DMSO-d6 at time 0.

	Day 0	**Day 7**	**Day 14**
PBS + solvent	H6 Peak Intensity celastrol in pure DMSO Day 0 / H6 Peak Intensity celastrol Day 0	H6 Peak Intensity celastrol in pure DMSO Day 0 / H6 Peak Intensity celastrol Day 0	H6 Peak Intensity celastrol in pure DMSO Day 0 / H6 Peak Intensity celastrol Day 0
100% DMSO-d6	1.00	1.08	1.09
50% DMSO-d6	1.33	2.70	5.00
10% DMSO-d6	4.76	3.84	4.76
5% DMSO-d6	11.10	10.00	12.50

Supplementary Table 2 | Stability test for celastrol in different solvents at day 0, day 7 and day 14 by LC-Q-TOF-MS. The stability is calculated based on the ratio between Peak Area internal standard (IS) divided by Peak Area celastrol[a]. Every experiment was repeated in duplicate.

	Day 0		**Day 7**		**Day 14**	
Solvent	Area IS/Area Celastrol Dilution (1:400)[b]	Area IS/Area Celastrol Dilution (1:800)[b]	Area IS/Area Celastrol Dilution (1:400)[b]	Area IS/Area Celastrol Dilution (1:800)[b]	Area IS/Area Celastrol Dilution (1:400)[b]	Area IS/Area Celastrol Dilution (1:800)[b]
Pure DMSO	1.70±0.04	1.77±0.02	2.11±0.16	2.48±0.18	2.53±0.02	2.61±0.05
50% DMSO	1.77±0.04	1.87±0.02	6.18±0.84	7.39±0.08	16.12±1.03	16.18±3.94
10% DMSO	2.75±0.2	2.96±0.08	6.16±0.88	6.41±1.53	12.69±1.1	14.03±3.11
5% DMSO	2.90±0.12	2.98±0.04	6.53±0.67	7.05±0.57	26.93±5.86	31.51±6.81
Cyclodextrin+DMSO[c]	3.47±0.15	3.91±0.62	2.40±0.19	2.39±0.3	3.61±0.43	3.86±0.47
Pure cyclodextrin[d]	8.25±0.28	8.90±0.71	3.53±0.28	5.06±1.90	5.44±0.21	6.39±1.75

[a] Initial concentration of celastrol 0.08 mg/mL

[b] The initial solution was diluted in H_2O:CH_3CN (1:1)

[c] 0.8 µL/mL DMSO + 45% PBS

[d] Cyclodextrin in 45% PBS